Available online at www.sciencedirect.com
ScienceDirect
Trans. Nonferrous Met. Soc. China 35(2025) 45−59
Transactions of Nonferrous Metals Society of China
www.tnmsc.cn

Microstructure evolution of 7050 aluminum forgings during surface cumulative plastic deformation

Jian-liang HU[1,2,3,4], Ze-xiong ZHANG[1,3,4], Cheng XING[1,3,4], Xiu-jiang WU[1,3,4], Shi-quan HUANG[2], Hong BO[5]

1. Key Laboratory of Advanced Forging & Stamping Technology and Science, Ministry of Education, Yanshan University, Qinhuangdao 066004, China;
2. State Key Laboratory of Precision Manufacturing for Extreme Service Performance, Central South University, Changsha 410083, China;
3. College of Mechanical Engineering, Yanshan University, Qinhuangdao 066004, China;
4. Hebei Engineering Technology Research Center of Metal Precision Plastic Processing, Yanshan University, Qinhuangdao 066004, China;
5. State Key Laboratory of Metastable Materials Science and Technology, Yanshan University, Qinhuangdao 066004, China

Received 24 May 2023; accepted 30 January 2024

Abstract: To elucidate the mechanisms of regulating the microstructure uniformity in 7050 aluminum forgings through surface cumulative plastic deformation (SCPD), the microstructure under different solution treatments was investigated using metallographic observation (OM), electron backscatter diffraction (EBSD), transmission electron microscopy (TEM), and X-ray diffraction (XRD). The findings demonstrate that the most uniform microstructure in the forgings is achieved with a solution treatment at 470 °C for 30 min. The SCPD process generates a significant number of needle-shaped precipitates, resulting in a higher dislocation density and stored energy. Solution treatments alleviate the pinning effect of second-phase particles and facilitate static recrystallization (SRX) in forgings, leading to a reduction in grain size. Additionally, mechanical testing results demonstrate 7%−13% increase in tensile strength and more uniform elongation of the forgings in different directions.

Key words: microstructure homogeneity; surface cumulative plastic deformation (SCPD); static recrystallization (SRX); dislocation density

1 Introduction

The 7000 series aluminum alloys have been widely applied to producing crucial structural components of large aircraft due to their excellent mechanical properties, particularly high specific strength [1,2]. Most large aircraft forgings exhibit a distinctive local structure with high reinforcement and thin walls [3]. However, traditional hot die forging conditions introduce a significant temperature gradient between the surface and core regions of the forging. This disparity can severely impact the performance of aerospace structural components, resulting in a substantial reduction in the utilization efficiency of aerospace materials [4,5].

In recent years, the research on the thermal deformation behavior of 7XXX aluminum alloy has attracted extensive attention. ZUO et al [6] successfully achieved fine crystals in 7055 aluminum alloy through a double-step hot rolling

Corresponding author: Hong BO, Tel: +86-335-8057031, E-mail: bohong@ysu.edu.cn
https://doi.org/10.1016/S1003-6326(24)66664-1

(DRT). Their further investigation revealed a substantial presence of $MgZn_2$ precipitation phase during the initial rolling, exerting a pinning effect on dislocations and grain boundaries. Subsequent short-term annealing alleviated this pinning effect, promoting the formation of numerous polygonal sub-grains and achieving grain refinement. HU et al [7] conducted surface cumulative plastic deformation (SCPD) on 7050 aluminum alloy and found that grain refinement primarily resulted from the accumulation of stored energy and dislocation density during the cumulative deformation process. Subsequently, they developed a static recrystallization (SRX) model for aluminum forgings to accurately describe the SRX behavior during SCPD. PADAP et al [8] performed solution treatments of 7075 aluminum alloy that had undergone uniaxial compression at 480 °C for 90 min. They observed a 4.54% reduction in alloy hardness after the treatments, accompanied by the appearance of $MgZn_2$ and Al_2CuMg precipitates, as revealed by X-ray diffraction. LIAO et al [9] conducted high strain rate rolling on 7050 aluminum alloy, leading to a high percentage of low-angle grain boundaries. This promoted the precipitation of the second-phase particles due to the presence of dislocations and sub-grains. The combination of high strain rate rolling and heat treatments resulted in the aluminum alloy with excellent properties, mainly attributed to the presence of precipitates and the second-phase particles. LI et al [10] investigated the micro-structure evolution of 7050 aluminum alloy under deformation at different temperatures. After the deformation at 350 °C, the microstructure transitioned from dislocation tangles to dislocation cells and sub-grains. At the deformation temperature of 450 °C, continuous dynamic recrystallization (DRX) occurred, with the primary nucleation mechanism being sub-grain growth and coalescence.

In this study, the SCPD process was proposed to address microstructure inhomogeneity in aluminum alloy forgings caused by traditional hot forging methods. The SCPD process aims to regulate the dislocation density on the surface of the forgings, and the subsequent solution treatments can promote recrystallization, refining the surface grains of the forgings. However, the microstructure evolution mechanism and its impact on mechanical properties during the SCPD process have not yet been clarified. In this study, the microstructure of SCPD under different solution treatments was investigated by metallographic observation (OM), electron backscattered diffraction (EBSD), transmission electron microscopy (TEM), and X-ray diffraction (XRD). Simultaneously, the mechanical performance tests were conducted to effectively characterize the improvement in the mechanical properties of the forgings by the SCPD process.

2 Experimental

2.1 SCPD experiment

The chemical compositions of 7050 aluminum alloy are given in Table 1.

Table 1 Chemical compositions of 7050 aluminum alloy billet (wt.%)

Zn	Mg	Cu	
7.37−7.69	1.16−2.42	2.46−2.64	
Si	Zr	Fe	Al
0.19−0.29	<0.14	<0.1	Bal.

To obtain forgings with an inhomogeneous microstructure, conventional hot-die forging experiments were performed using a 3 MN hydraulic press at 350 °C. The experimental schematic is shown in Fig. 1(a), with a pressing velocity of 0.02 m/s and a deformation amount of 10%. The initially formed forging is shown in Fig. 1(b). According to the metallographic images of the surface and core microstructures of the forging, the average grain diameter of the surface is about 105 μm and the average grain diameter of the core is about 83 μm.

The inhomogeneous H-shaped forging obtained from the hot die forging was heated to 200 °C and held for 40 min, and then the same molds were heated to 300 °C using a thermocouple, and the SCPD experiments were conducted under this condition. The finally formed forging is shown in Fig. 1(c). After the experiment, the deformed samples were treated with solution treatments at 470 °C and held for 10, 30, 40, and 60 min, respectively. Finally, samples were taken at the position shown in Fig. 1(c) for metallographic observation (OM). The samples were polished with

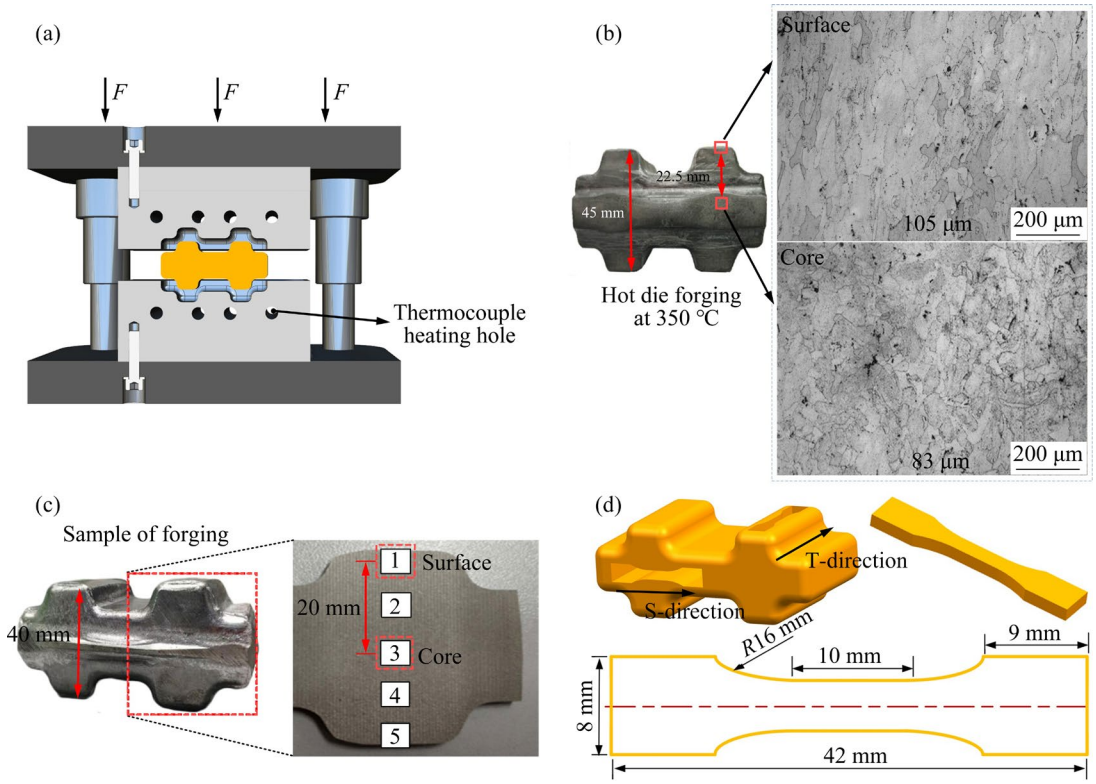

Fig. 1 Experimental schematic of SCPD process: (a) Die forging mold; (b) Conventional hot die forging at 350 °C; (c) SCPD experimental die forgings at 300 °C and sampling locations; (d) Sampling chart for mechanical property testing

different grades of SiC grinding paper and then eroded using an etchant composed of 1 mL HF, 2 mL HNO_3, 2 mL HCl and 95 mL H_2O. To further characterize the grain structure, the samples were electrochemically polished at −15 °C with a voltage of 20 V. The electrolyte used was a composition of 10 vol.% perchloric acid ($HClO_4$) and 90 vol.% methanol (CH_3OH) solution. Subsequently, electron backscatter diffraction (EBSD) experiments were performed on the Sigma 500 scanning electron microscope. The sample of 3 mm in diameter was electropolished using 30 vol.% nitric acid (HNO_3) solution and 70 vol.% methanol (CH_3OH) solution in an RL-I dual-jet thinning instrument. The voltage used was 14−18 V, and the temperature was maintained at −20 °C. Transmission electron microscopy (TEM) observation was conducted on a Talos F200X transmission electron microscope with an acceleration voltage of 200 kV. X-ray diffraction examination was performed on a D/max2500 PC X-ray diffractometer, operating at 40 kV with a copper target. The scanning wavelength (λ) was 1.5406 Å, and the scanning range was set from 30° to 50°, employing a step scan mode with a step width of 2 s and a step size of 0.02°.

2.2 Mechanical performance experiment

To investigate the influence of the SCPD experiments on the homogeneity of 7050 aluminum forgings, mechanical performance testing was conducted by using an INSTRON-8801 fatigue testing machine. The clamping force was 1.38 MPa, and the tensile rate was quasi-static at 0.0001 m/s. The forgings obtained from the SCPD experiment were sampled in the rib direction (T-direction) and thickness direction (S-direction) at a mold temperature of 300 °C, as shown in Fig. 1(d). For comparison, the forgings obtained from the hot die forging experiment at 350 °C were subjected to the same sampling process. Subsequently, the obtained samples were subjected to heat treatments of (470 °C, 1 h) + (121 °C, 6 h) + (177 °C, 12 h). Finally, the tensile strength, and elongation of these samples were measured through tensile testing.

3 Results and discussion

3.1 Grain structure evolution of forgings

The metallographic images in Fig. 2 illustrate the grain structure evolution of the surface and core of the forging after different solution treatments.

The results show that a more significant recrystallization occurs internally. When the solution treatment time is only 10 min, as shown in Figs. 2(a, b), the degree of recrystallization is low due to the short solution treatments, and the energy inside the forging is not fully released, resulting in larger grain size. With a solution treatment for 30 min, as shown in Figs. 2(c, d), the surface of the forging undergoes more obvious recrystallization, with a significant decrease in grain size. The average grain diameter of the surface is about 79 μm, while the average grain diameter of the core is about 76 μm. The grain sizes in both zones significantly decrease, resulting in improved microstructure homogeneity of the forging. With a solution treatment for 60 min, as shown in Figs. 2(e, f), the grain structure of the surface remains unchanged, while the grain size in the core continues to increase.

3.2 Microstructure evolution of forgings

Figure 3 shows the EBSD images of 7050 aluminum forgings after SCPD and different solution treatments. It can be observed that the coarse deformed grains of the forgings are separated by low-angle boundaries and refined significantly. The surface of forgings is mainly composed of fine sub-grains and a small portion of coarse deformed grains, while the number of sub-grains decreases and the number of recrystallized grains increases in the core region compared to the surface.

As shown in Figs. 3(a, b), with a solution treatment time of 10 min, the strain energy released on the surface can only support a small portion of

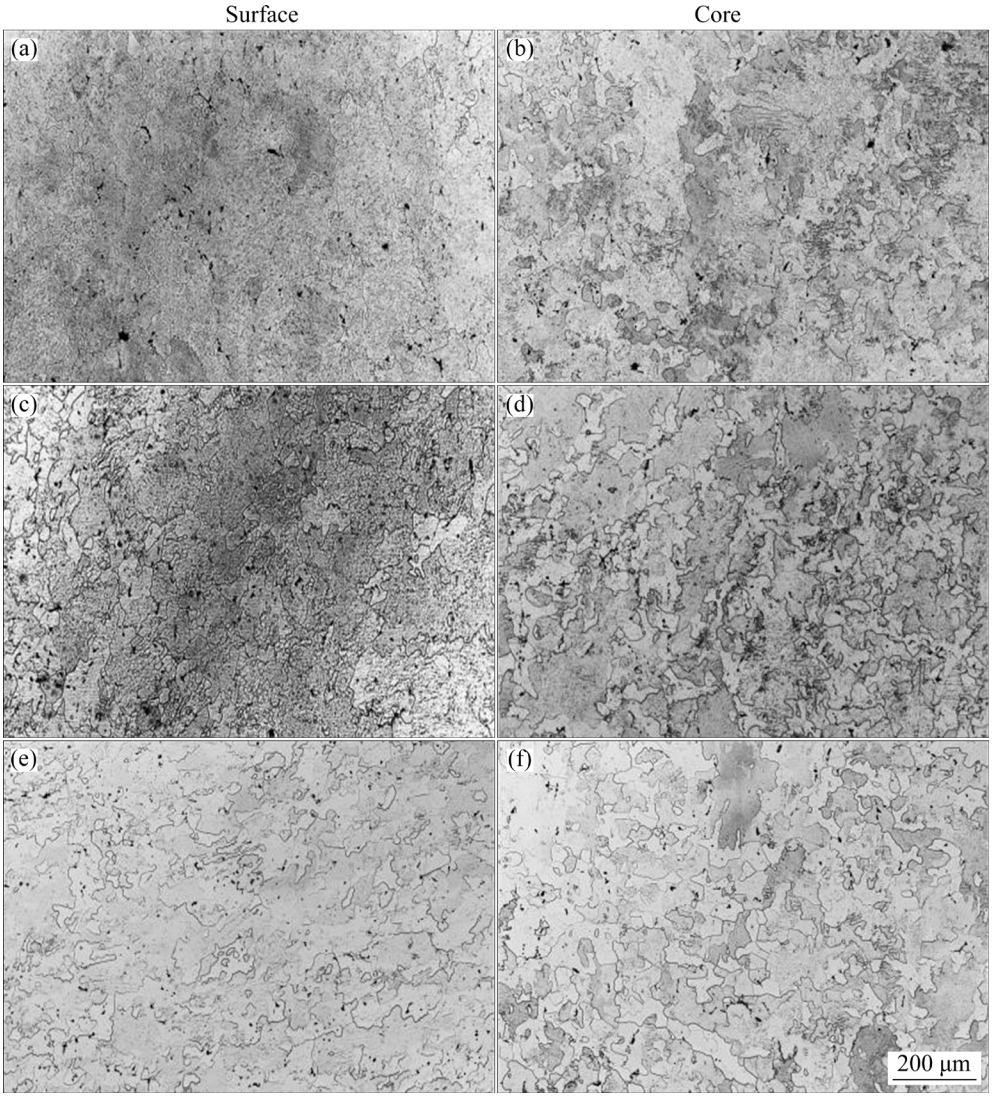

Fig. 2 Metallographic images of aluminum forgings after SCPD and solution treatment at 470 °C for different durations: (a, b) 10 min; (c, d) 30 min; (e, f) 60 min

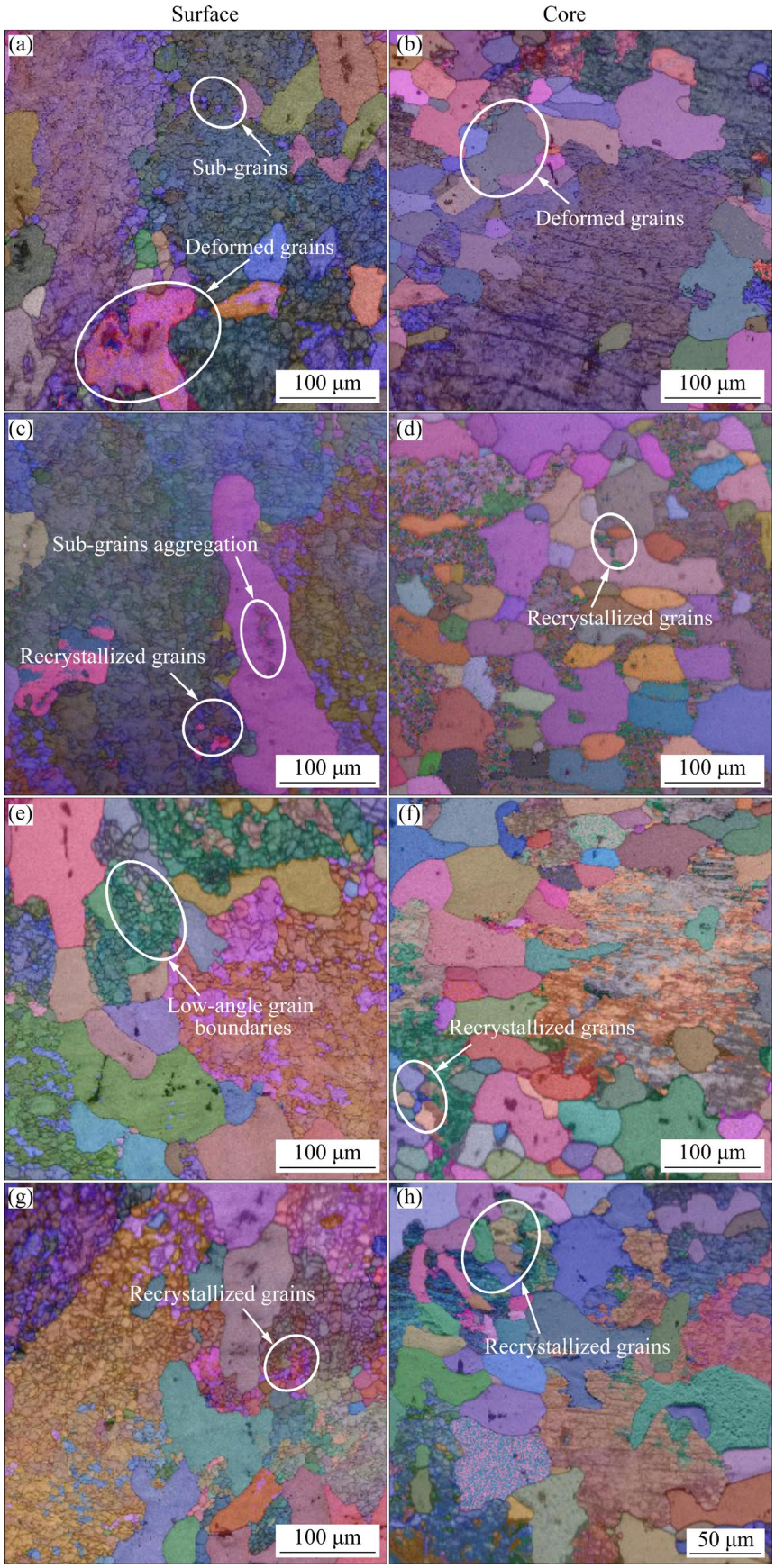

Fig. 3 EBSD images of 7050 aluminum forgings after SCPD and solution treatment at 470 °C for different durations: (a, b) 10 min; (c, d) 30 min; (e, f) 40 min; (g, h) 60 min

grains to undergo recrystallization, and most sub-grains remain. There is not enough driving force to form recrystallized grains. Therefore, the surface has a higher content of sub-grains. In the central region of the forgings, due to the higher deformation rate, a significant static recrystallization (SRX) phenomenon occurs earlier during the solution treatments, resulting in a higher number of recrystallized grains [11]. As shown in Fig. 4(a), a higher proportion of large grains and larger grain sizes are observed. When the solution time is 30 min, the aggregation of sub-grains occurs inside the coarse deformed grains on the surface, as shown in Figs. 3(c, d). These sub-grains continuously absorb energy and transform into the large-angle grain boundaries, forming the recrystallization nuclei [12]. These low-angle grain boundaries separate the larger deformed grains, leading to a decrease in average grain size and degree of grain refinement [13], and a significant increase in the number of recrystallized grains in the core zone. As shown in Fig. 4(b), the proportion of small grains increases, improving the microstructure uniformity of forgings. As the solution treatment time increases to 40 min, the accumulated strain energy inside the forgings is further released, but recrystallized grains begin to grow prematurely, as shown in Fig. 4(c). With a solution treatment for 60 min, the accumulated strain energy inside the forgings is fully released, and the trend grain size distribution is similar to that for 40 min.

Figure 5 depicts the distribution of the misorientation angles for different solution treatments conditions after the SCPD process. In this study, only data with orientation angles higher than 2.5° were considered [14]. As shown in Fig. 5, the proportion of low-angle grain boundaries (f_{LAGBs}) in the microstructure of the forging surface are higher than that in the core, indicating a higher proportion of sub-grains on the surface. In the SCPD experiment, the cumulative deformation of the forging surface is less than that of the core. During the subsequent solution treatments, the strain energy released on the surface is insufficient to support the formation of recrystallized grains, and most of the grains remain as sub-grains.

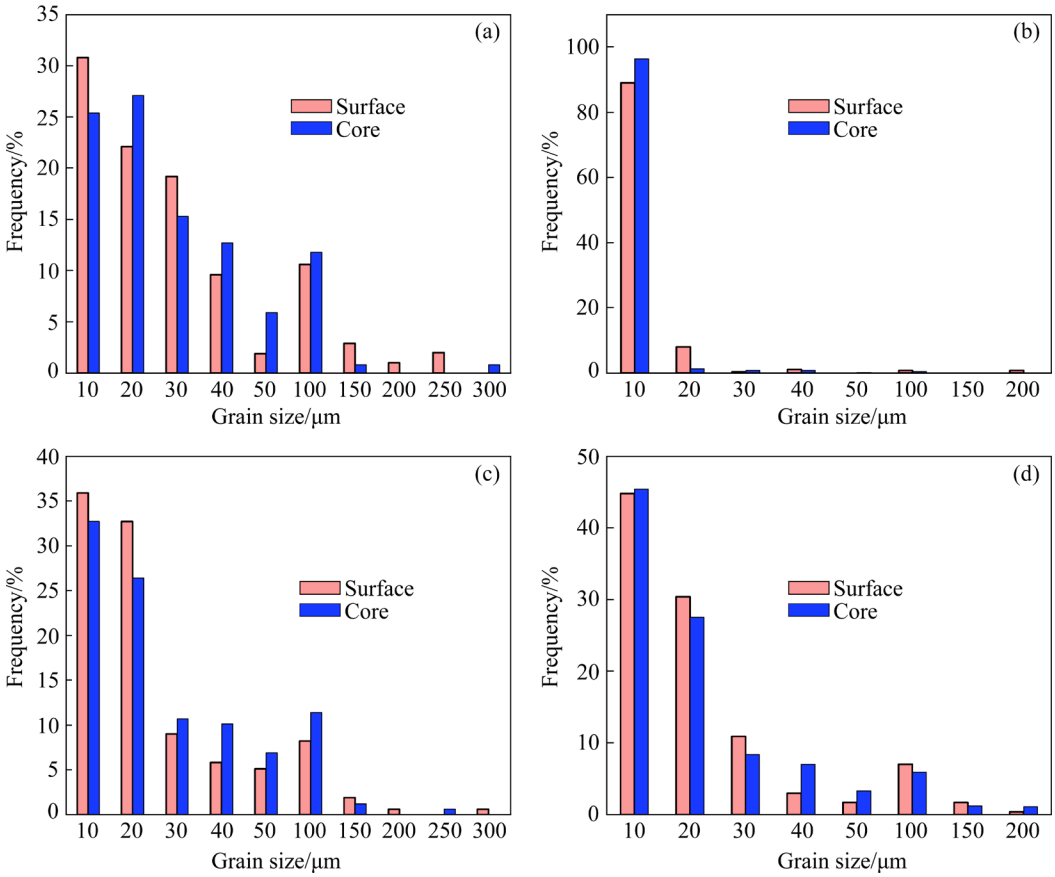

Fig. 4 Histogram of grain size distribution of 7050 aluminum forgings after SCPD and solution treatment at 470 °C for different durations: (a) 10 min; (b) 30 min; (c) 40 min; (d) 60 min

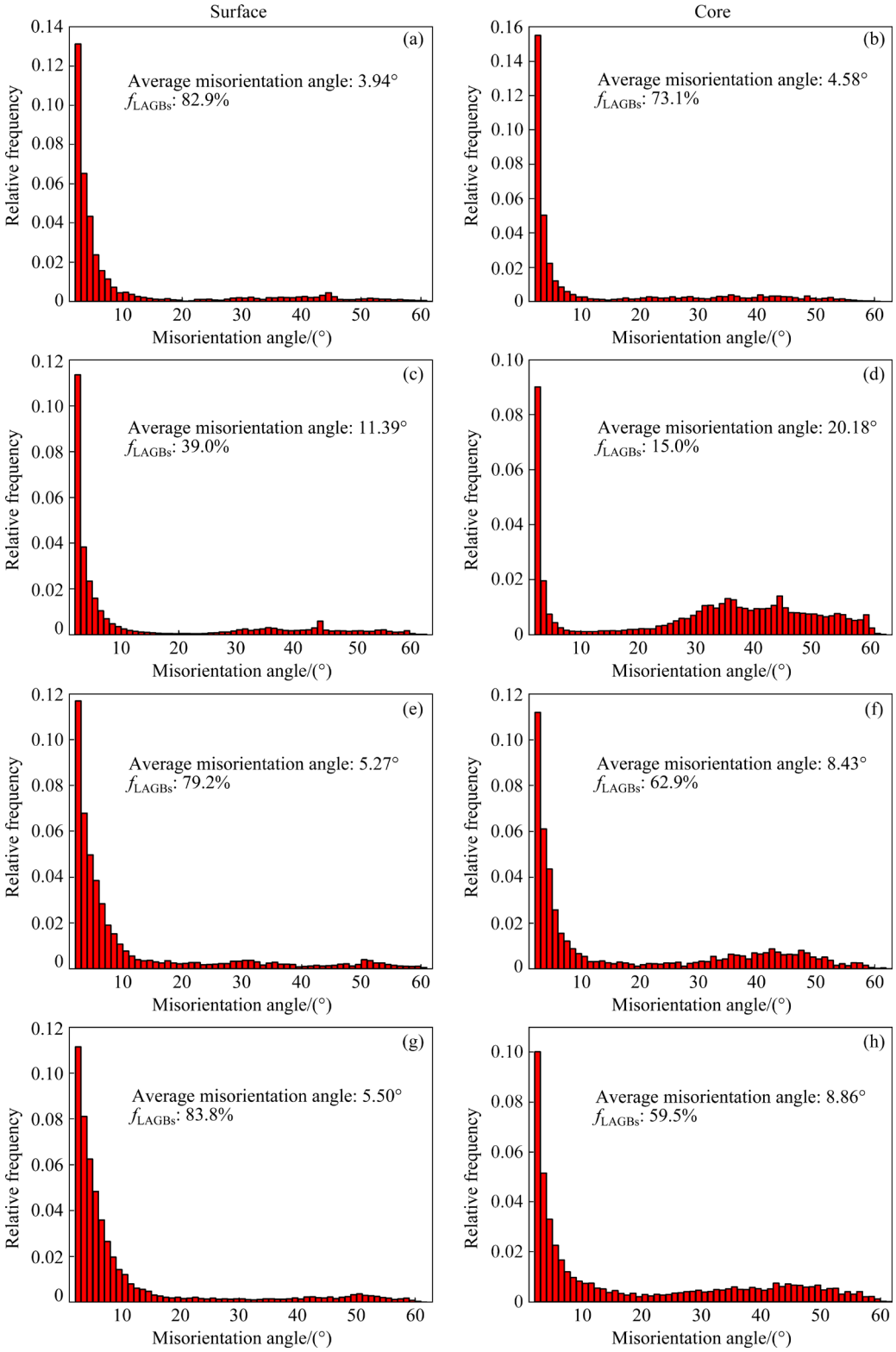

Fig. 5 Misorientation angle distributions of 7050 aluminum forgings after SCPD and solution treatment at 470 °C for different durations: (a, b) 10 min; (c, d) 30 min; (e, f) 40 min; (g, h) 60 min

At the solution treatment time of 10 min, the f_{LAGBs} values in the surface and core of the forging are 82.9% and 73.1%, respectively. However, with an increase in solution treatment time to 30 min, the f_{LAGBs} values in the surface and core decrease to 39.0% and 15.0%, respectively. As the solution treatment time increases, the proportion of low-angle grain boundaries decreases, and the average

misorientation angle increases to 11.39° and 20.18°, indicating that the number of large-angle grain boundaries increases and the degree of recrystallization is enhanced. The distribution of low-angle and large-angle grain boundaries in the forging exhibits a bimodal pattern, and the transition from low-angle to large-angle grain boundaries is continuous, indicating that low-angle grain boundaries are gradually transformed into large-angle grain boundaries. At a solution treatment of 40 min, the f_{LAGBs} values in the surface and core of the forging are 79.2% and 62.9%, respectively. As the stored strain energy is gradually released, static recrystallization (SRX) is gradually completed, and the distribution of low-angle and large-angle grain boundaries in the core of the forging becomes unimodal, with the majority of low-angle grain boundaries converting to large-angle grain boundaries. At a solution time of 60 min, the f_{LAGBs} values in the surface and core of the forging are 83.8% and 59.5%, respectively. Both the surface and core of the forging exhibit a unimodal distribution of low-angle and large-angle grain boundaries, indicating the complete conversion from low-angle to large-angle grain boundaries, and the grains begin to grow during recrystallization.

Figure 6 illustrates the distribution of recrystallization and deformation zones in both the surface and core of forgings under different solution treatments. By comparing the recrystallization distribution of the forging, it can be observed that the proportion of the blue zone in the surface is lower than that in the core for different solution treatments, indicating that the degree of recrystallization in the surface is lower than that in the core. This difference is evidently related to the degree of deformation and stored deformation energy in both the surface and core of the forging [15].

With an increase in solution treatment time, the proportion of the red zone in the forging gradually decreases, indicating a reduction in the deformation zones and a significant increase in the recrystallization zones. Meanwhile, the proportion of the substructure zone in the yellow zone exhibits an initial increase followed by a subsequent decrease. During the early stage of solution treatments, numerous residual dislocations in the microstructure continuously transform into sub-grains through high-temperature thermal activation, serving as nucleation centers of recrystallization. These centers steadily increase in size through migration or coalescence mechanisms [16]. With the increase of solution treatment time, these recrystallization nucleation centers grow into new recrystallized grains, and some substructure zones also transform into recrystallized zones. Consequently, the proportion of substructure zones gradually decreases, while the proportion of recrystallized zones increases.

According to the statistical analysis of EBSD data (Fig. 7), the proportion of recrystallized and sub-structured zones in the surface and core of aluminum forgings varies with solution treatment time. Specifically, with duration of 10 min, the total proportions of recrystallized and sub-structured zones in the surface and core of the forging are 49.2% and 47.2%, respectively. Extending the duration to 30 min leads to an increase of the total proportion to 52.6% in the surface and 79.9% in the score. However, with a further increase to 40 min, the total proportion of recrystallized and sub-structured zones in the surface slightly rises to 57.0%, while it decreases slightly to 73.6% in the core. Finally, with 60 min solution treatment, the proportions of recrystallized and sub-structured zones in the surface and core remain relatively stable at 57.4% and 74.7%, respectively.

These results suggest that the energy stored from internal deformation in the aluminum forging is completely released after 40 min of solution treatments. Further increasing the duration of the solution treatment does not yield a significant improvement in the microstructure through internal recrystallization. The degree of recrystallization exhibits little change between 30 and 40 min. Based on the findings discussed above, it is concluded that the optimal solution treatment duration for enhancing the microstructure uniformity of the aluminum forgings is 30 min.

3.3 Mechanism evolution of forgings

Dislocation is a common type of line defects in deformable materials and represents an important form of energy stored [17,18]. The initial form of dislocations is primarily a mass of tangled dislocation lines. As the internal energy of the material is gradually released, the dislocation density decreases. During the process of polygonization,

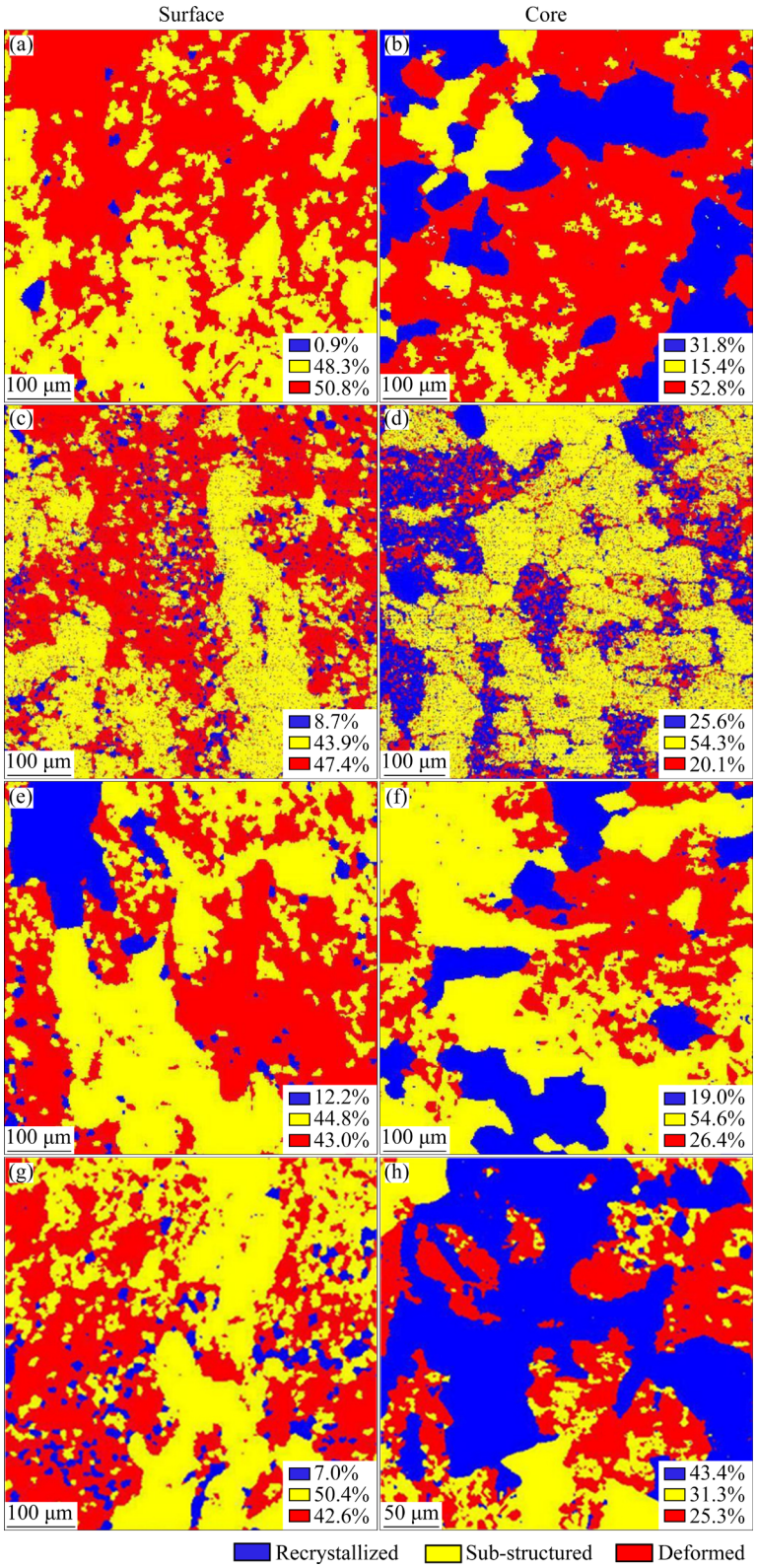

Fig. 6 Distribution of recrystallization in aluminum forgings after SCPD and solution treatment at 470 °C for different durations: (a, b) 10 min; (c, d) 30 min; (e, f) 40 min; (g, h) 60 min

the randomly entangled dislocations start to organize into hexagonal arrangements, forming the dislocation cells. Subsequently, the walls of the dislocation cells gradually thin out [19]. Finally, the dislocation cells merge and transform into sub-grains, which serve as nucleation sites for recrystallization.

To further analyze the morphology of dislocations,

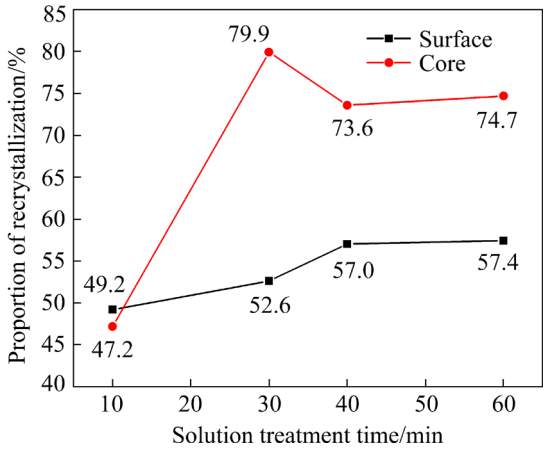

Fig. 7 Recrystallization degree of forgings after SCPD and different solution treatments

TEM images of aluminum forgings obtained in SCPD experiments are shown in Fig. 8. It can be seen that there are many precipitates in the microstructure of the forgings. The second-phase particles of different sizes and shapes pin dislocations, preventing their climb and cross-slip [20]. This results in a higher concentration of dislocations and increased deformation stored-energy in the forgings. Moreover, upon examining the microstructure of the forging shown in Fig. 8, a notable presence of dislocations is observed. The majority of dislocations are intertangled, while some exhibit a tendency to form dislocation cells. Figure 8(b) highlights the existence of sub-grains in the core of the forgings. These sub-grains are featured by small size and unclear boundaries. A comparison of the TEM images of the surface and core reveals a slightly higher dislocation density in the core region.

Figure 9 presents the TEM images illustrating the surface and core microstructures of the SCPD specimens subjected to different solution treatments. A comparison with the forgings in Fig. 8 reveals a notable decrease in both the number and size of the second-phase particles with increasing solution treatment duration. With 10 min solution treatment, a certain amount of second-phase particles remain in the microstructure, hindering the movement of dislocations and the migration of sub-grains and grain boundaries [21]. This results in elevated dislocation content in the forgings, as shown in Figs. 9(a, b). With a prolonged solution treatment to 30 min, most second-phase particles re-dissolve into the matrix, and the remaining particles become significantly finer, weakening their hindering effect on dislocations and sub-grains boundaries, as shown in Figs. 9(c, d). Finally, when the solution treatment time is extended to 60 min, almost all the second-phase particles dissolve into the matrix, as shown in Figs. 9(e, f).

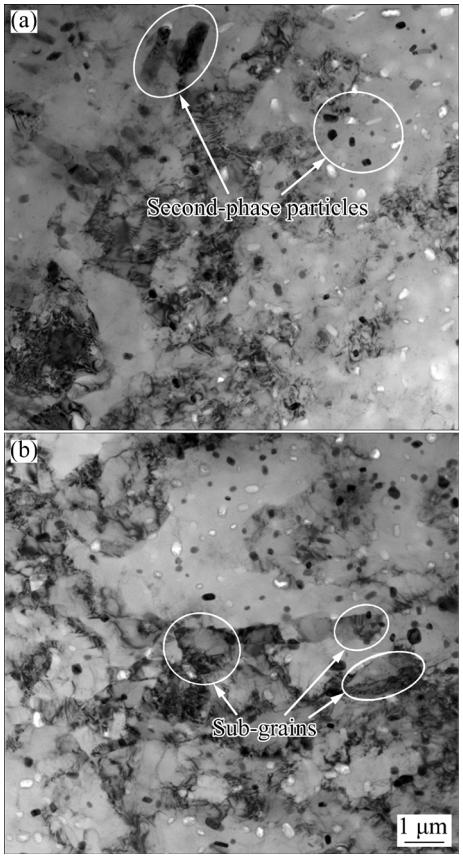

Fig. 8 TEM images of aluminum forgings after SCPD: (a) Surface; (b) Core

The dislocation morphology and density of forgings vary with different solution treatments. As shown in Fig. 9(a), when the solution treatment time is 10 min, the surface of the forgings displays a higher dislocation density. This is characterized by the fuzzy sub-grain boundaries containing longitudinal and transverse dislocation lines, rather than disordered and tangled dislocation lines. The dislocation morphology in the core of forgings is similar to that in the surface, as shown in Fig. 9(b). More sub-grains are generated in the core, with adjacent sub-grains merging and growing. At this point, the sub-grain boundaries are formed by several parallel dislocation lines, and clear dislocation lines begin to appear within the sub-grains. Additionally, adjacent sub-grain boundaries have not completely disappeared [22].

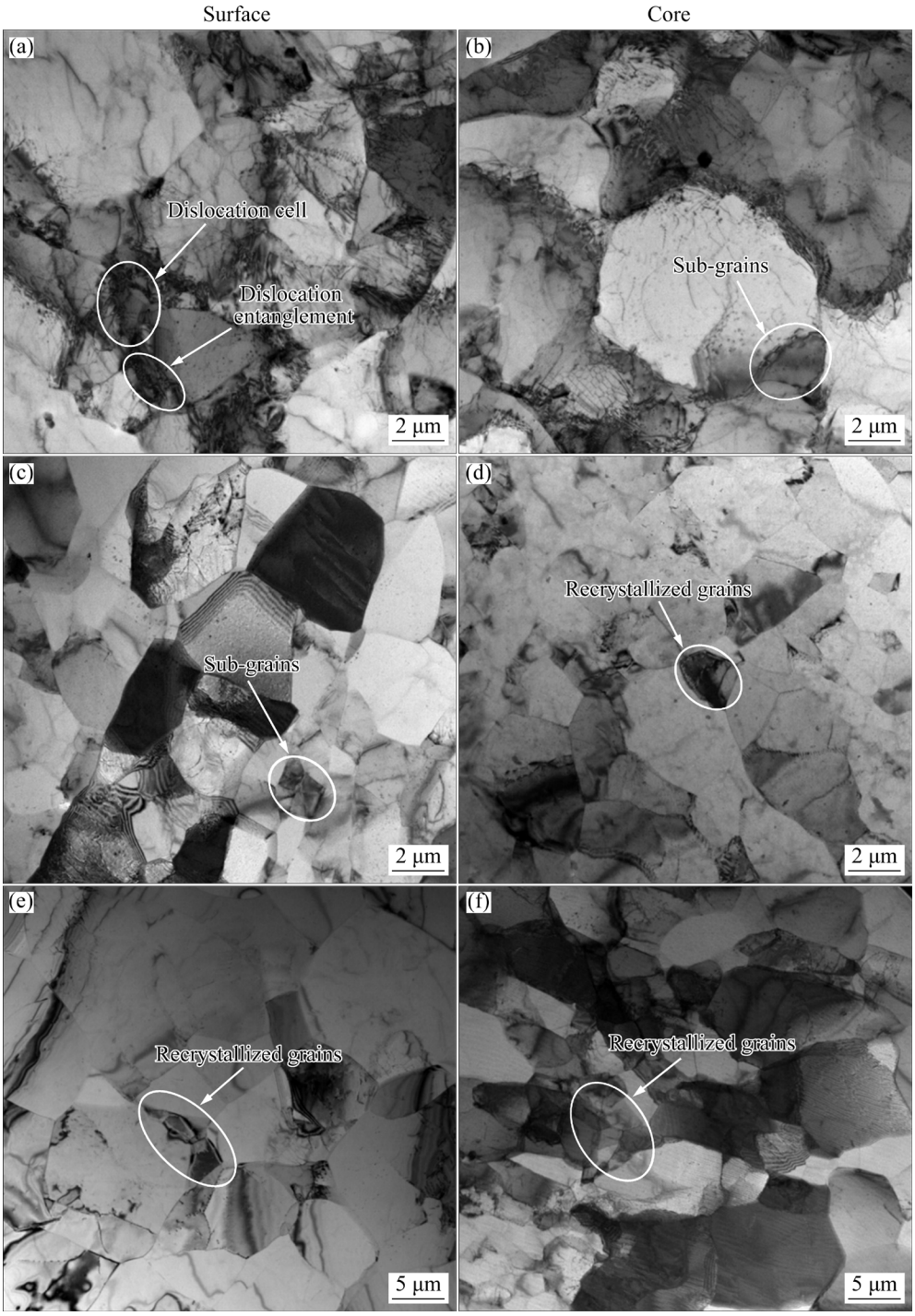

Fig. 9 TEM images of aluminum forgings after SCPD and solution treatment at 470 °C for different durations: (a, b) 10 min; (c, d) 30 min; (e, f) 60 min

When the solution treatment is prolonged to 30 min, a significant reduction in dislocation density is observed, accompanied by the emergence of a large number of sub-grains. As shown in Fig. 9(c), these sub-grains are featured by larger sizes, and straighter and clearer boundaries [23]. However, dislocation lines remain within a small number of sub-grains. As shown in Fig. 9(d), the dislocation morphology of the core of the forgings is similar to that of the surface. The microstructure reveals a considerable presence of large-sized sub-grains, with their boundaries gradually transforming into large-angle grain boundaries [24].

With the extension of the solution treatment

time to 60 min, the dislocation morphology in both the surface and core of the forging is shown in Figs. 9(e, f). Almost all the deformation stored-energy in the forgings is released, resulting in a significant reduction in dislocation density. Meanwhile, there is a substantial increase in the number of sub-grains, which improves the recrystallization nucleation process, giving rise to the formation of new recrystallized grains [25]. Further extension of the solution treatment time can lead to continued growth in the size of recrystallized grains in the forgings, which is not conducive to achieving the overall homogeneity in the microstructure of aluminum forgings.

In general, the TEM images shown in Fig. 9 indicate that the solution treatment has a significant effect on the microstructure of the SCPD aluminum forgings. With an increase in the solution treatment time, both the number and size of the second-phase particles decrease, weakening their hindrance to dislocations and sub-grains boundaries. The dislocation morphology evolves from tangled dislocation lines to clear sub-grain boundaries. Meanwhile, the formation and growth of large sub-grains become apparent, and the nucleation process of recrystallization is completed, leading to the formation of new recrystallized grains. Therefore, the careful selection of solution treatments is crucial for effectively controlling the microstructure and properties of SCPD aluminum forgings.

The X-ray diffraction technique was employed to obtain the diffraction pattern of forgings under different deformation conditions. Fourier analysis was then utilized to calculate the dislocation density values in both the surface and core of the forgings under different deformation conditions [26], as shown in Fig. 10. It is evident that SCPD increases the dislocation density in both the surface and cores of the forgings. Specifically, the dislocation density of the surface increases by about 8%, from 1.13×10^{14} to $1.22\times10^{14}\,m^{-2}$, while the dislocation density of the core increases by about 6%, from 1.51×10^{14} to $1.6\times10^{14}\,m^{-2}$. Therefore, the SCPD process elevates the overall deformation stored-energy within the aluminum forging, with the surface experiencing greater increase in deformation stored-energy. However, it is noteworthy that the highest overall deformation stored-energy remains in the core of the forgings.

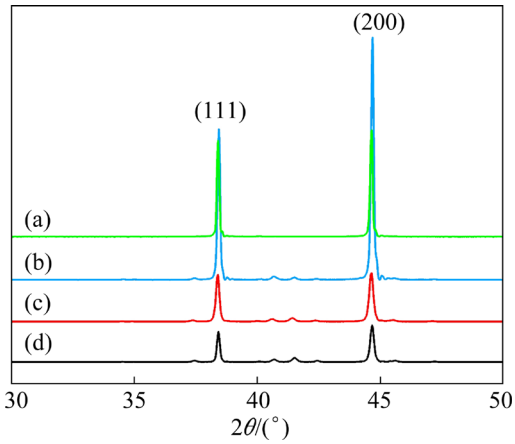

Fig. 10 X-ray diffraction patterns under different deformation conditions: (a) Core of forgings after SCPD; (b) Surface of forgings after SCPD; (c) Core of hot die forgings; (d) Surface of hot die forgings

3.4 Mechanical performance

A comparison of the stress−strain curves obtained from SCPD process and the hot die forging process, as shown in Figs. 11(a, b), reveals that during the initial stages of plastic deformation, the flow stress of the specimen experiences a rapid increase with rising strain. This surge is attributed to the multiplication and entanglement of dislocations induced by plastic deformation, impeding the motion of dislocations. The results suggest that the SCPD process significantly improves tensile strength.

As shown in Figs. 11(a, b), the SCPD-treated forged specimen exhibits substantially increase in both the strength and plasticity in the T-direction, whereas there is a significant increase in strength and a reduction in plasticity in the S-direction. This suggests that SCPD improves the plasticity of the surface. The subsequent heat treatment induces static recrystallization (SRX) in the forgings, resulting in finer and more uniform grain sizes and ultimately achieving refinement and strengthening [27]. In the T-direction, the elongation of surface and core is increased from 7.12% and 6.13% to 10.75% and 8.56%, respectively, while the tensile strength is decreased by 8.6% and 10.3%. In the S-direction, both the surface and core tensile strengths are significantly increased, while plasticity is decreased. The elongation is decreased from 11.59% and 11.72% to 10.21% and 9.78%, respectively, while the tensile strength is decreased by 7.2% and 11.9%. This is attributed to the

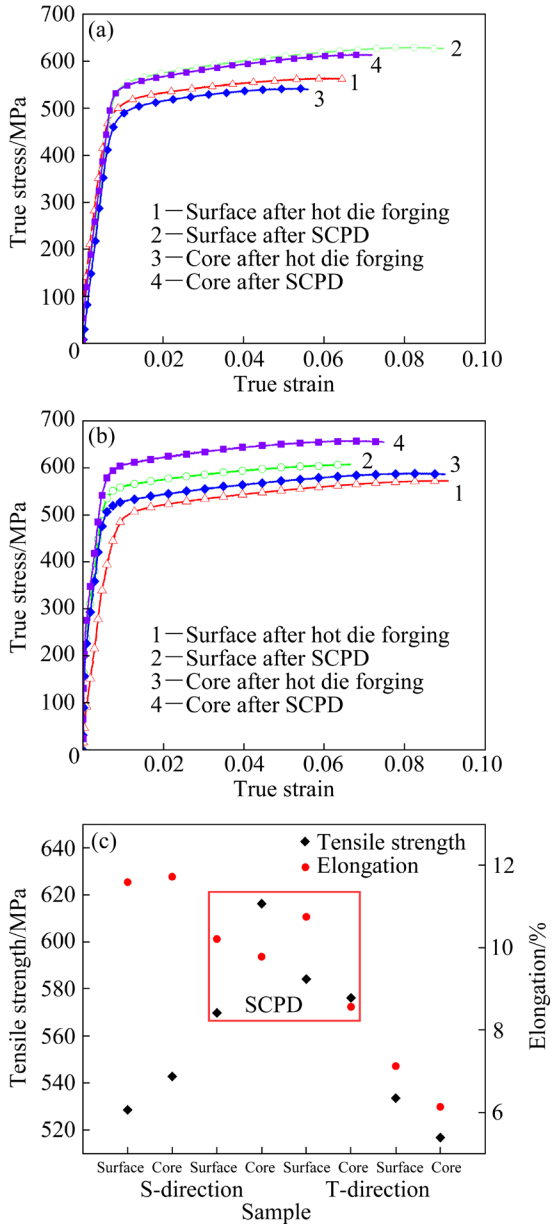

Fig. 11 Mechanical properties of specimens under different deformation conditions: (a) True stress−true strain curves of T-direction samples; (b) True stress−true strain curves of S-direction samples; (c) Tensile strength and elongation of samples

excessively fine grain size at the sampling location in the S-direction, leading to higher yield strength than tensile strength, thus increasing the yielding-to-tensile ratio [28]. Figure 11(c) presents the results of the mechanical performance tests, revealing a maximum tensile strength with SCPD of 616.25 MPa. By comparing the results of hot die forging with those of SCPD, it is evident that the SCPD process effectively enhances the mechanical performance of the forgings.

4 Conclusions

(1) The combination of SCPD and solution treatment at 470 °C for 30 min achieves a uniform average grain size in the surface and core of the forging, thus resulting in excellent microstructure uniformity.

(2) The SCPD process changes the content and size of the precipitation phases inside the forging by regulating the dislocation density in the surface. The solution treatments release deformation stored-energy, thereby promoting static recrystallization (SRX) in the forging and refining the grain size in the surface to achieve uniformity regulation. Additionally, with the increase in solution treatment time, the number of sub-grains and recrystallized grains in the forging gradually increases. The recrystallization degree is lower in the surface than that in the core.

(3) By SCPD and solution treatments, the tensile strength of the forgings increased by 7%−13%. The rib elongation is increased from 7.12% to 10.75% for the surface and from 6.13% to 8.56% for the core. Excessive grain refinement and dislocation motion reduce the web elongation, from 11.59% to 10.21% for the surface and from 11.72% to 9.78% for the core. More uniform mechanical properties of the forgings are achieved.

CRediT authorship contribution statement

Jian-liang HU: Conceptualization, Methodology, Funding acquisition, Writing − Review & editing; **Ze-xiong ZHANG:** Data curation, Formal analysis, Writing − Original draft; **Cheng XING:** Visualization, Investigation; **Xiu-jiang WU:** Resources, Validation; **Shi-quan HUANG:** Supervision, Project administration; **Hong BO:** Conceptualization, Funding acquisition, Resources, Supervision.

Declaration of competing interest

The authors declare that they have no known competing financial interests or personal relationships that could have appeared to influence the work reported in this paper.

Acknowledgments

This work was supported by the Natural Science Foundation of Hebei Province, China (Nos. E2019203075, E2021203059), the National Natural Science Foundation of China (No. 52171018), Top Young Talents Project of the Education Department of

Hebei Province, China (No. BJ2019001), and the Open Research Fund of State Key Laboratory of Precision Manufacturing for Extreme Service Performance, Central South University, China (No. Kfkt2023-09).

References

[1] ROMETSCH P A, ZHANG Yong, KNIGHT S. Heat treatment of 7xxx series aluminum alloys—Some recent developments [J]. Transactions of Nonferrous Metals Society of China, 2014, 24(7): 2003−2017. https://doi.org/10.1016/s1003-6326(14)63306-9.

[2] CHEN Guo-liang, CHEN Ming-he, WANG Ning, SUN Jia-wei. Hot forming process with synchronous cooling for AA2024 aluminum alloy and its application [J]. International Journal of Advanced Manufacturing Technology, 2016, 86(1/2/3/4): 133−139. https://doi.org/10.1007/s00170-015-8170-3.

[3] ZHANG Jian-sheng, WU Dao-xiang, ZHOU Jie, WANG Jing. Multi-objective optimization of process parameters for 7050 aluminum alloy rib-web forgings precise forming based on taguchi method [J]. Procedia Engineering, 2014, 81: 558−563. https://doi.org/10.1016/j.proeng.2014.10.039.

[4] HU Jian-liang, WU Xiu-jiang, BO Hong, JIAO Zi-teng, HUANG Shi-quan, JIN Miao. Dislocation density model and microstructure of 7A85 aluminum alloy during thermal deformation [J]. Journal of Central South University, 2021, 28(10): 2999−3007. https://doi.org/10.1007/s11771-021-4832-5.

[5] SHE Xin-wei, JIANG Xian-quan, WANG Pu-quan, TANG Bin-bin, CHEN Kang, LIU Yu-jie, CAO Wei-nan. Relationship between microstructure and mechanical properties of 5083 aluminum alloy thick plate [J]. Transactions of Nonferrous Metals Society of China, 2020, 30(7): 1780−1789. https://doi.org/10.1016/s1003-6326(20) 65338-9.

[6] ZUO Jin-rong, HOU Long-gang, SHI Jin-tao, CUI Hua, ZHUANG Lin-zhong, ZHANG Ji-shan. The mechanism of grain refinement and plasticity enhancement by an improved thermomechanical treatment of 7055 Al alloy [J]. Materials Science and Engineering A, 2017, 70242−70252. https://doi.org/10.1016/j.msea.2017.06.106.

[7] HU jian-liang, ZHAO Zi-han, DONG Meng-xiao, WANG Huan, JIN Miao, HUANG Shi-quan, BO Hong. Microstructure homogeneity regulation of 7050 aluminum forgings by surface cumulative plastic deformation [J]. Transactions of Nonferrous Metals Society of China, 2022, 32(9): 2814−2827. https://doi.org/10.1016/s1003-6326(22) 65985-5.

[8] PADAP A K, YADAV A P, KUMAR P, KUMAR N. Effect of aging heat treatment and uniaxial compression on thermal behavior of 7075 aluminum alloy [J]. Materials Today−Proceedings, 2020, 335442−335447. https://doi.org/10.1016/j.matpr.2020.03.196.

[9] LIAO Yang, YAN Hong-ge, XIA Wei-jun, CHEN Ji-hua, SU Bin, LI Xin-yu, ZHAO Lu. Effect of heat treatment on the microstructure and properties of high strain rate rolled 7050 aluminum alloy [J]. Metals and Materials International, 2022, 28(4): 1014−1025. https://doi.org/10.1007/s12540-020-00961-w.

[10] LI Jun-peng, SHEN Jian, YAN Xiao-dong, MAO Bai-ping, YAN Liang-ming. Microstructure evolution of 7050 aluminum alloy during hot deformation [J]. Transactions of Nonferrous Metals Society of China, 2010, 20(2): 189−194. https://doi.org/10.1016/s1003-6326(09)60119-9.

[11] DING Hong-bo, LIU Qiang, ZHOU Hai-tao, ZHOU Xiao, ATRENS A. Effect of thermal-mechanical processing on microstructure and mechanical properties of duplex-phase Mg−8Li−3Al−0.4Y alloy [J]. Transactions of Nonferrous Metals Society of China, 2017, 27(12): 2587−2597. https://doi.org/10.1016/s1003-6326(17)60286-3.

[12] WANG Qing-hang, JIANG Bin, TANG Ai-tao, FU Jie, JIANG Zhong-tao, SHENG Hao-ran, ZHANG Ding-fei, HUNAG Guang-sheng, PAN Fu-sheng. Unveiling annealing texture formation and static recrystallization kinetics of hot-rolled Mg−Al−Zn−Mn−Ca alloy [J]. Journal of Materials Science and Technology, 2020, 43(8): 104−118. https://doi.org/10.1016/j.jmst.2020.01.018.

[13] CHEN Yan-xia, YANG Yan-qing, Feng Zong-qiang, ZHAO Guang-ming, HUANG Bin, LUO Xian, ZHANG Yu-sheng, ZHANG Wei. Microstructure, microtexture and precipitation in the ultrafine-grained surface of an Al−Zn−Mg−Cu alloy processed by sliding friction treatment [J]. Materials Characterization, 2017, 123189−123197. https://doi.org/10.1016/j.matchar.2016.11.021.

[14] COURTAS S, GREGOIRE M, FEDERSPIEL X, BICAIS-LEPINAY N, WYON C. Electron back scattered diffraction (EBSD) use and applications in newest technologies development [J]. Microelectronics Reliability, 2006, 46(9/10/11): 1530−1535. https://doi.org/10.1016/j. microrel.2006.07.031.

[15] LENG Jin-feng, REN Bing-hui, ZHOU Qing-bo, ZHAO Ji-wei. Effect of Sc and Zr on recrystallization behavior of 7075 aluminum alloy [J]. Transactions of Nonferrous Metals Society of China, 2021, 31(9): 2545−2557. https://doi.org/10.1016/S1003-6326(21)65674-1.

[16] MA Cun-qiang, HOU Long-gang, ZHANG Ji-shan, ZHUANG Lin-zhong. Influence of thickness reduction per pass on strain, microstructures and mechanical properties of 7050 Al alloy sheet processed by asymmetric rolling [J]. Materials Science and Engineering A, 2016, 650: 454−468. https://doi.org/10.1016/j.msea.2015.10.059.

[17] SONG Yang, ZHANG Zhi-ming, WANG Kai, LI Hong-xu, ZHU Zi-zong. Effects of extrusion processing on microstructure of 7075Al alloy in the semi-solid state [J]. Journal of Wuhan University of Technology, 2019, 34(6): 1433−1443. https://doi.org/10.1007/s11595-019-2210-z.

[18] ZHONG Li-wei, GAO Wen-Li, FENG Zhao-hui, LU Zheng ZHU Cong-cong. Hot deformation characterization of as-homogenized Al−Cu−Li X2A66 alloy through processing maps and microstructural evolution [J]. Journal of Materials Science and Technology, 2019, 35(10): 2409−2421. https://doi.org/10.1016/j.jmst.2019.06.001.

[19] REN X D, ZHANG Y K, RUAN L, JIANG D W, ZHANG T, CHEN K M. Effect of laser shock processing on the fatigue crack initiation and propagation of 7050-T7451 aluminum alloy [J]. Materials Science and Engineering A, 2011, 528(6): 2899−2903. https://doi.org/10.1016/j.msea.2010.12. 058.

[20] XU Li-juan, ZHENG Yun-fei, LIANG Zhen-quan, HAN Shi-wei, XUE Xiang, XIAO Shu-long, TIAN Jing, CHEN

Yu-yong. Creep behavior and microstructure evolution of titanium matrix composites reinforced with TiB, TiC and Y_2O_3 [J]. Transactions of Nonferrous Metals Society of China, 2023, 33(2): 467−480. https://doi.org/10.1016/s1003-6326(22)66120-x.

[21] HUO Wang-tu, HOU Long-gang, LANG Yu-jing, CUI Hua, ZHUANG Lin-zhong, ZHANG Ji-shan. Improved thermo-mechanical processing for effective grain refinement of high-strength AA7050 Al alloy [J]. Materials Science and Engineering A, 2015, 626: 86−93. https://doi.org/10.1016/j.msea.2014.12.071.

[22] YANG Jun-zhou, WU Jian-jun, XIE Hai-nan, LI Zhi-guo, WANG Kai-wei. Mechanism of continuous dynamic recrystallization of Ti−6Al−4V alloy during superplastic forming with sub-grain rotation [J]. Transactions of Nonferrous Metals Society of China, 2023, 33(3): 777−788. https://doi.org/10.1016/s1003-6326(23)66145-x.

[23] LIU Wen-yi, ZHAO Huan, LI Dan, ZHANG Zhi-qing, HUANG Guang-jie, LIU Qing. Hot deformation behavior of AA7085 aluminum alloy during isothermal compression at elevated temperature [J]. Materials Science and Engineering A, 2014, 596: 176−182. https://doi.org/10.1016/j.msea.2013.12.012.

[24] SHEN Tong, FAN Cai-he, HU Ze-yi, WU Qin, CHEN Yu-zhou. Effect of strain rate on microstructure and mechanical properties of spray-formed Al−Cu−Mg alloy [J]. Transactions of Nonferrous Metals Society of China, 2022, 32(4): 1096−1104. https://doi.org/10.1016/S1003-6326(22)65879-5.

[25] FIELD D P, BEHRENS L, ROOT J M. Identification of particle stimulated nucleation during recrystallization of AA 7050 [J]. CMC-computers Materials and Continua, 2009, 14(3): 171−183. https://doi.org/10.3970/cmc.2009.014.171.

[26] ZHAO Zi-han, HU Jian-liang, XING Cheng, WANG Huan, JIN Miao, HUANG Shi-quan. Microstructural evolution and regulation of inhomogeneized 7050 aluminum alloy during compression at low temperature [J]. Journal of Materials Engineering and Performance, 2024, 33: 7960−7974. https://doi.org/10. 1007/s11665-023-08494-0.

[27] TIAMIYU A A, TARI V, SZPUNAR J A, ODESHI A G, KHAN A K. Effects of grain refinement on the quasi-static compressive behavior of AISI 321 austenitic stainless steel: EBSD, TEM, and XRD Studies [J]. International Journal of Plasticity, 2018, 107: 79−99. https://doi.org/10.1016/j.ijplas.2018.03.014.

[28] JIA P F, CAO Y H, GENG Y D, HE L Z, XIAO N, CUI J Z. Effects of d. c. current on the phase transformation in 7050 alloy during homogenization[J]. Materials Characterization, 2014, 9621−9627. https://doi.org/10.1016/j.matchar.2014.07.017.

7050 铝合金锻件在表层增塑累积变形中的显微组织演变

胡建良[1,2,3,4]，张泽雄[1,3,4]，邢 程[1,3,4]，吴秀江[1,3,4]，黄始全[2]，薄 宏[5]

1. 燕山大学 先进锻压成形技术与科学教育部重点实验室，秦皇岛 066004；
2. 中南大学 极端服役性能精准制造国家重点实验室，长沙 410083；
3. 燕山大学 机械工程学院，秦皇岛 066004；
4. 燕山大学 河北省金属精密塑性加工工程技术研究中心，秦皇岛 066004；
5. 燕山大学 亚稳态材料科学与技术国家重点实验室，秦皇岛 066004

摘 要：为了揭示表层增塑累积变形调控 7050 铝合金锻件显微组织均匀性的微观机理，采用金相显微镜、扫描电镜、透射电子显微镜和 X 射线衍射仪等对不同固溶处理模锻件的显微组织进行研究。结果表明，在 470 ℃固溶处理 30 min 可获得最均匀的显微组织。通过表层增塑累积变形工艺可以产生大量针状析出相，实现位错密度和形变储能的累积，结合后续的固溶处理工艺，减轻第二相粒子的钉轧作用，使锻件发生静态再结晶，从而减小晶粒尺寸。同时，力学性能测试结果表明，表层增塑累积变形处理的模锻件抗拉强度提高 7%~13%，伸长率也更加均匀。

关键词：显微组织均匀性；表层增塑累积变形；静态再结晶；位错密度

(Edited by Bing YANG)